Case Studies in Thermal Engineering 22 (2020) 100726

Contents lists available at ScienceDirect

Case Studies in Thermal Engineering

journal homepage: http://www.elsevier.com/locate/csite

Significances of blowing and suction processes on the occurrence of thermo-magneto-convection phenomenon in a narrow nanofluidic medium: A revised Buongiorno's nanofluid model

M. Zaydan [a], A. Wakif [a,*], I.L. Animasaun [b], Umair Khan [c], Dumitru Baleanu [d,e,f], R. Sehaqui [a]

[a] Laboratory of Mechanics, Faculty of Sciences Aïn Chock, University Hassan II of Casablanca, Casablanca, 20000, Morocco
[b] Fluid Dynamics and Survey Research Group, Department of Mathematical Sciences, Federal University of Technology, Akure, Nigeria
[c] Department of Mathematics and Social Sciences, Sukkur IBA University, Sukkur, 65200, Sindh, Pakistan
[d] Department of Mathematics, Cankaya University, 06790, Ankara, Turkey
[e] Institute of Space Sciences, 077125, Magurele, Romania
[f] Department of Medical Research, China Medical University Hospital, China Medical University, Taichung, 40447, Taiwan

ARTICLE INFO

Keywords:
Linear stability
Nanofluid
Magnetic field
Throughflow
Spectral method

ABSTRACT

In this numerical examination, the thermal stability of an electrically conducting nanofluid is deliberated comprehensively by considering the presence of an externally applied magnetic field along with an imposed vertical throughflow. Additionally, this thin nanofluidic layer is supposed to have a Newtonian rheological behavior, heated from below, and confined horizontally between two permeable rigid plates of infinite extension. Herein, the governing conservation equations are strengthened realistically by the revised version of the Buongiorno's mathematical model, in which the vertical component of the mass flux of solid nanoparticles is presumed to vanish entirely at the horizontal permeable boundaries. After specifying the basic state of the present nanofluid problem, the linear stability theory and normal mode analysis technique are applied properly to obtain the principal stability equations. Finally, the eigenvalue problem derived analytically is tackled thereafter numerically via the Chebyshev-Gauss-Lobatto Spectral Method (CGLSM), in which the thermal Rayleigh number is chosen as an eigenvalue. As a main result, it was demonstrated that the throughflow effect exhibits a dual behavior on the complex dynamics of the system. However, the excreted magnetic field has always a stabilizing impact on the nanofluidic medium.

1. Introduction

The significance of the magnetic field on the motion of electrically conducting liquids can be described as a broad area of interest in fluid mechanics with so many open questions. The record shows that the concept is the fundamental basis of the invention of the electromagnetic pump by Rossow [1] in the year 1918. Whenever an electrically conducting substance is subjected to a constant magnetic field, an electromotive force (e.m.f.) and Lorentz force are generated physically. Consequently, the production of an electric current is inevitable. Alfvén [2] remarked that due to the magnetic field, the electric current also generates mechanical forces capable

* Corresponding author.
E-mail addresses: wakif.abderrahim@gmail.com, abderrahim.wakif-etu@etu.univh2c.ma (A. Wakif).

https://doi.org/10.1016/j.csite.2020.100726
Received 11 May 2020; Received in revised form 14 July 2020; Accepted 19 July 2020
Available online 27 July 2020

of changing the dynamics of the flowing fluid. Pal and Kumar [3] explained the importance of a uniform magnetic field on Rayleigh-Bernard convection flows of low Prandtl number. It was observed that a stronger magnetic field is capable of causing chaotic flow. A better description of the effect of the magnetic forces on the behavior of fluid parcels within a continuous medium is articulated by Bulatova et al. [4]. Sheikholeslami and Rokni [5] deliberated on the dynamics of heat transfer convection within the laminar flow of Newtonian nanofluids by introducing the ferrohydrodynamic (FHD) and magnetohydrodynamic (MHD) notions. The significance of Lorentz force on the flow of non-Newtonian blood flow with magnetic nanoparticles in a stenosed artery, the dynamics of cupric-water nanofluid flow in a porous channel, on the flow of Jeffrey fluid, and the motion of three-dimensional nanofluid on a convectively heated stretchable surface are discussed comprehensively by Mirza et al. [6], Sheikholeslami [7], Ahmad, A. Ishak [8], and Hayat et al. [9]. In another study, the problem of time-dependent mixed convection flow of micropolar fluid on a vertical porous surface subject to Lorentz forces, mass, and thermal diffusions was presented by Ibrahim et al. [10]. It was observed that the velocity of the transport phenomenon within the boundary layer decreases with an increase in the magnetic field strength. Kandasamy et al. [11] presented the problem of chemical reaction, buoyancy, and Lorentz forces on the flow of Newtonian fluids over a thermally stratified surface. It is shown that a decrease in the horizontal velocity with an increase in temperature distribution is foreseeable due to an increase in the magnitude of Lorentz forces. This leads Sivaraj et al. [12] to study the thermal performance of nanofluids by studying the flow of 29 nm copper oxide-based water nanofluid through a magnetic field and an electric field. It was shown that when the Hall effect is considerably large, a higher magnitude of horizontal velocity and cross-flow are guaranteed. The characterstics of nanofluid flows through a magnetic field situated on an upper horizontal surface of a paraboloid of revolution in the presence of a quartic kind of autocatalytic chemical reaction was elaborated by Makinde and Animasaun [13,14]. In these reports, the variable magnetic field was adopted due to the thickness of the object. Keeping in mind the importance of using nanofluids in the heat transfer enrichment in many industrial applications, several engineering flow problems were recently scrutinized by Das et al. [15] and Acharya et al. [16–20].

Later on, Buongiorno [21] developed a non-homogenous mixture model, which is proposed especially for nanofluids to facilitate the examination of heat and mass transportations in nanofluidic media based on viable strong theories and many realistic assumptions. This innovative nanofluid model includes explicitly the important role of Brownian motion and thermophoresis phenomenon that can be happened for the nanoparticles inside a fluidic medium at the nanoscale dimension under certain external physical constraints. Since the statement of the Buongiorno's two-phase nanofluid model in 2006, numerous further proposals have been reported thereafter by Nield and Kuznetsov [22–24] to predict approximately the probable criterion for the appearance of natural convective nanofluid flows driven in a confined nanofluidic non-porous/porous medium under the adjusted influence of an imposed negative temperature gradient applied vertically between two permeable/impermeable horizontal boundaries in the case where the vertical mass flux of nanoparticles is supposed to have vanished on these limiting horizontal boundaries, in which the volumetric fractions of these nano-sized chemical species are controlled passively at the boundaries by considering them among the local unknowns of the nanofluid problem. In this framework, Wakif et al. [25] conducted a comprehensive numerical spectral analysis on the temporal evolution of MHD convective Couette flows along with their thermal and mass features for radiative copper-based water nanofluids in the cases of the single and two-phase nanofluid models. To gain more understanding of the mechanisms leading to this expected thermal enhancement, Animasaun et al. [26] and Wakif et al. [27] deliberated thoroughly the impact of thermo-migration mechanism driven by tiny particles as well as their haphazard motion on the dynamical and physical characteristics of nanofluidic systems.

Despite the recent widespread usage of the revised two-phase nanofluid model as a more realistic physical approach to adopt in the modeling of a huge number of convective nanofluid flow problems, the dealing with the assumption of zero nanoparticles mass flux condition in the nanofluid stability problems is still scientifically questionable and should be open to further scrutiny because it was ill-posed as well along with the linear stability theory in the methodological mathematical sense to determine the stability parameters accurately via the Classical Galerkin Weighted Residuals Technique (CGWRT) as described in Refs. [22–24]. An inclusive survey on this topic was first reported by Wakif et al. [28] in 2016 when they had examined analytically and numerically the electroconvection stability in a rotating porous medium filled by a dielectric nanofluid. After two years, this remarkable finding was re-confirmed comprehensively by Wakif et al. [29] in another nanofluid stability problem by utilizing several innovative computational methods, like Power Series Method (PSM), Classical Galerkin Weighted Residuals Technique (CGWRT), Wakif-Galerkin Weighted Residuals Technique (WGWRT), Polynomial Collocation Method (PCM), Runge-Kutta-Fehlberg Method (RKFM) and Chebyshev-Gauss-Lobatto Spectral Method (CGLSM). From the methodological point of view, it was demonstrated extensively (i.e., semi-analytically and numerically) that CGWRT is strictly incapable to tackle correctly the thermal stabilities in a confined nanofluidic medium with the assumption of zero nanoparticles mass flux condition and provides unacceptable findings, because of its higher deviation in the precision of physical results compared with the aforesaid executed methods. Notwithstanding the much attention paid in the above-cited literature survey to the examination of thermal stabilities in confined nanofluidic media, but there are even still exist some computational unpredictabilities since the most commonly used CGWRT semi-analytical method can not assure reliable physical results for the nanofluid stability problems with the passive control of nanoparticles on the boundaries, which open a vast challenge in research to develop robustness methods possessing an excellent capability to predict the manifestation of thermal instabilities in nanofluids under the Nield's boundary conditions [22,23] with a higher level of correctness. Motivating by the surviving lack in this bullish research topic as well as by the countless useful applications of nanofluids in many advanced areas and technological sophistical processes, the present comprehensive analysis aims to shed light on the significance of a uniform upward/downward throughflow (i.e., blowing and suction effects) on the thermal criterion for the onset of thermo-magneto-convection phenomena that can take place in horizontal confined nanofluidic media under the impact of a negative temperature gradient applied vertically on the nanofluidic layer in the presence on an external uniform magnetic field. By adopting the assumption of zero nanoparticles mass flux condition at the isothermal permeable walls along with the modified Maxwell's equations, the Buongiorno's two-phase nanofluid model was improved physically by incorporating the convective contribution of solid nanoparticles in the thermal energy equation

besides the Brownian motion and the thermophoresis processes as reported in Ref. [24]. After applying an approprtiate non-dimensionalization procedure on the stated conservation equations, the stationary stability equations were derived via the proper use of linear stability theory and normal mode analysis technique. In this stage, the resulting ordinary differential equations along with their appropriate boundary conditions were rearranged mathematically and then discretized spatially by utilizing a suitable spectral collocation method, whose results are validated broadly with those of other methods in some special cases. Accordingly, to examine the thermal stability of the studied nanofluidic medium, the linear discrete system was written in the form of a linear eigenvalue problem by selecting the thermal Rayleigh number as its eigenvalue.In this regards, the influences of different involved physical parameters are discussed properly via several tabular and graphical representations.

2. Mathematical formulation

As presented schematically in Fig. 1, an infinite nanofluidic layer of depth L is heated isothermally from below via an imposed negative temperature gradient $(T_C - T_H)/L$ and exposed horizontally under the effect of a uniform gravitational field $\mathbf{g} = -g\mathbf{e_z}$, where T_H and $T_C(<T_H)$ are the temperatures at the lower and upper boundaries, respectively. Additionally, the confined nanofluidic medium is supposed to be incompressible, has a Newtonian rheological behavior, electrically conducting, surrounded by an unvarying vertical magnetic field $\mathbf{H_0} = H_0\mathbf{e_z}$ and subjected to a constant upward/downward velocity $\mathbf{V_0} = w_0\mathbf{e_z}$ at the rigid permeable boundaries located spatially at $z^* = 0$ and $z^* = L$, where w_0 is chosen to take a positive value for the blowing flow control case, whereas it is negative for the suction situation. As a physical constraint, the isothermal permeable walls are supposed to be not crossed transversely by any mass flux J^*_{Sz} of nanoparticles. A Cartesian coordinate system (x^*, y^*, z^*) is selected along with the unit vectors $(\mathbf{e_x}, \mathbf{e_y}, \mathbf{e_z})$ to facilitate the mathematical description of the present nanofluid flow configuration. Moreover, the thermophysical properties of the nanofluid (i.e., viscosity, thermal conductivity, specific heat, magnetic permeability, and electrical conductivity) are assumed to remain constant in the vicinity of the reference temperature T_H of the hot wall, except for the density in the momentum equation, which is done formally by the Oberbeck-Boussinesq approximation. Furthermore, the asterisk symbolizations are used in the mathematical formulation to distinguish absolutely the dimensional variables/unknowns X^* from their corresponding non-dimensional varieties X.

2.1. Governing equations

Under the aforementioned assumptions, the relevant conservation equations characterizing the magnetohydrodynamic convective motion of the electrically conducting nanofluid are stated as follows [24,30–32]:

$$\nabla^*.\mathbf{V}^* = 0, \tag{1}$$

$$\rho_0\left[\frac{\partial \mathbf{V}^*}{\partial t^*} + (\mathbf{V}^*.\nabla^*)\mathbf{V}^*\right] = -\nabla^* P^* + \mu\nabla^{*2}\mathbf{V}^* + \rho\mathbf{g} + \frac{\mu_e}{4\pi}(\nabla^* \times \mathbf{H}^*) \times \mathbf{H}^*, \tag{2}$$

$$\rho = \rho_S\varphi_0 + (1-\varphi_0)\rho_0[1-\beta(T^* - T_H)], \tag{3}$$

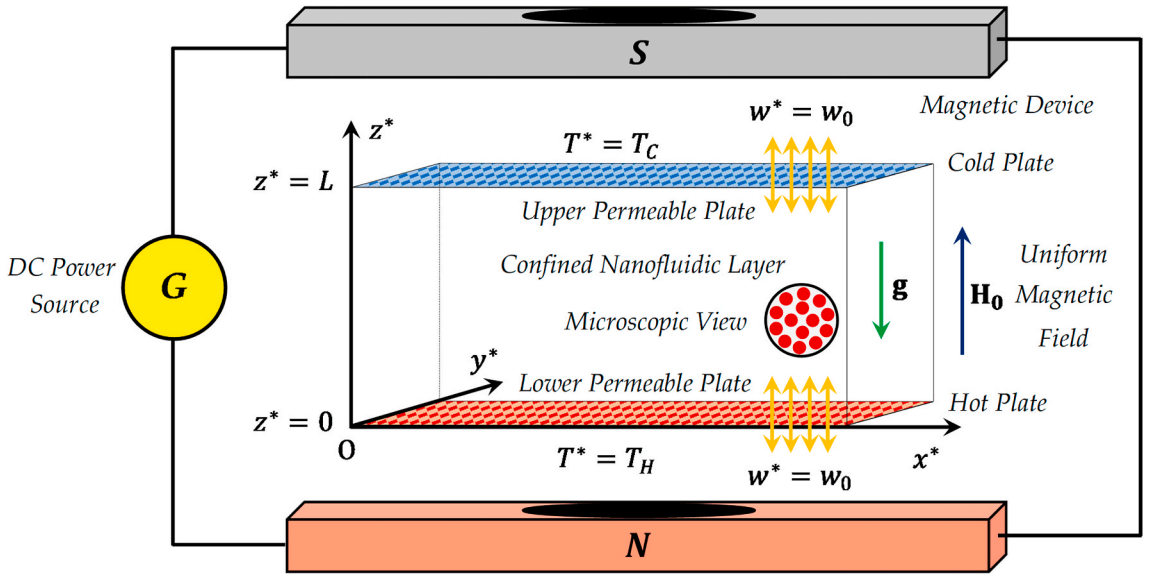

Fig. 1. Geometrical configuration of the nanofluid stability problem.

$$\frac{\partial T^*}{\partial t^*} + (\mathbf{V}^*.\nabla^*)T^* = \frac{k}{(\rho C_P)}\nabla^{*2}T^* + \frac{(\rho C_P)_S}{(\rho C_P)}\left[D_B\nabla^*\varphi^* - (\varphi^* - \varphi_0)\mathbf{V}^* + \left(\frac{D_T}{T_H}\right)\nabla^*T^*\right]\nabla^*T^*, \tag{4}$$

$$\frac{\partial \varphi^*}{\partial t^*} + (\mathbf{V}^*.\nabla^*)\varphi^* = D_B\nabla^{*2}\varphi^* + \left(\frac{D_T}{T_H}\right)\nabla^{*2}T^*, \tag{5}$$

$$\nabla^*.\mathbf{H}^* = 0, \tag{6}$$

$$\frac{\partial \mathbf{H}^*}{\partial t^*} + (\mathbf{V}^*.\nabla^*)\mathbf{H}^* = (\mathbf{H}^*.\nabla^*)\mathbf{V}^* + \eta\nabla^{*2}\mathbf{H}^*. \tag{7}$$

Here, $\mathbf{V}^*\left(=(u^*,v^*,w^*)\right)$ represents the vector velocity, t^* highlights the dimensional time, $\rho_0\left(=\rho(T_H)\right)$ marks the reference value of the nanofluid density, P^* symbolizes the pressure, μ, ρ and k designate the dynamic viscosity, the density and the thermal conductivity of the nanofluid, respectively, ρ_S shows the density of nanoparticles, β refers to the thermal expansion coefficient of the nanofluid, T^* denotes the dimensional temperature, φ^* indicates the local volume fraction of nanoparticles, φ_0 means the initial volume fraction of nanoparticles, (ρC_P) and $(\rho C_P)_S$ stands for the heat capacitance of nanofluid and solid nanoparticles, respectively, $\alpha\left(=k/(\rho C_P)\right)$ characterizes the thermal diffusivity of the nanofluid, $\mathbf{H}^*\left(=\left(H_x^*,H_y^*,H_z^*\right)\right)$ signifies the magnetic field, $\nabla^*\left(=(\partial/\partial x^*, \partial/\partial y^*, \partial/\partial z^*)\right)$ defines mathematically the vector differential operator, μ_e specifies the magnetic permeability of the medium, $\eta\left(=(4\pi\mu_e\sigma)^{-1}\right)$ expresses the magnetic diffusivity of the nanofluid and σ illustrates the nanofluid electrical conductivity.

For isothermal permeable rigid plates with the vanishing nanoparticles mass flux condition, the appropriate boundary conditions are written as follows:

$$\begin{cases} w^* = w_0,\ \dfrac{\partial w^*}{\partial z^*} = 0,\ J_{Sz}^* = 0,\ T^* = T_H \ \text{ at } \ z^* = 0, \\ w^* = w_0,\ \dfrac{\partial w^*}{\partial z^*} = 0,\ J_{Sz}^* = 0,\ T^* = T_C \ \text{ at } \ z^* = L. \end{cases} \tag{8}$$

Further, the nanoparticles mass flux vector $\mathbf{J}_\mathbf{S}^*\left(=\left(J_{Sx}^*,J_{Sy}^*,J_{Sz}^*\right)\right)$ and its vertical component $J_{Sz}^*\left(=\mathbf{J}_\mathbf{S}^*.\mathbf{e_z}\right)$ are given by Nield and Kuznetsov [24] as:

$$\mathbf{J}_\mathbf{S}^* = -\rho_S\left[D_B\nabla^*\varphi^* + \left(\frac{D_T}{T_H}\right)\nabla^*T^* - (\varphi^* - \varphi_0)\mathbf{V}^*\right], \tag{9}$$

$$J_{Sz}^* = -\rho_S\left[D_B\frac{\partial\varphi^*}{\partial z^*} + \left(\frac{D_T}{T_H}\right)\frac{\partial T^*}{\partial z^*} - (\varphi^* - \varphi_0)w^*\right] \tag{10}$$

By assuming that the horizontal boundaries are electrically non-conducting, so there is no effective current flow can cross these boundaries to the exterior region. Also, the induced magnetic field $\mathbf{H}^*$ is continuous at the boundaries with the external magnetic field $\mathbf{H_0}$. Consequently, the following additional boundary conditions can be considered [33,34]:

$$(\nabla^* \times \mathbf{H}^*)\mathbf{e_z} = 0 \ \text{ and } \ \left(H_x^*,H_y^*,H_z^*\right) = (0,0,H_0) \ \text{ at } \ z^* = 0,L. \tag{11}$$

By invoking Eq. (6), the above magnetic boundary conditions reduce to:

$$H_x^* = H_y^* = \frac{\partial H_z^*}{\partial z^*} = 0\ ,\ H_z^* = H_0 \ \text{ at } \ z^* = 0,L. \tag{12}$$

Moreover, the non-dimensionalization procedure can be applied properly by including the following dimensionless variables:

$$\begin{cases} (x,y,z) = \dfrac{1}{L}\ (x^*,y^*,z^*),\ t = \left(\dfrac{\alpha}{L^2}\right)t^*,\ \mathbf{V} = \left(\dfrac{L}{\alpha}\right)\mathbf{V}^*,\ P = \left(\dfrac{L^2}{\rho_0\,\alpha^2}\right)P^*,\ T = \dfrac{T^* - T_C}{T_H - T_C}, \\ \varphi = \dfrac{\varphi^* - \varphi_0}{\varphi_0},\ J_{zS} = \left(\dfrac{L}{\rho_S D_B\varphi_0}\right)J_{zS}^*,\ \left(H_x,H_y,H_z\right) = \dfrac{1}{H_0}\left(H_x^*,H_y^*,H_z^*\right) \end{cases} \tag{13}$$

Therefore, Eqs. (1)–(7) are altered to the following dimensionless forms:

$$\nabla.\mathbf{V} = 0, \tag{14}$$

$$\frac{\partial \mathbf{V}}{\partial t} + (\mathbf{V}.\nabla)\mathbf{V} = -\nabla[P + \mathrm{Pr}(R_M + Ra)z] + \mathrm{Pr}\nabla^2\mathbf{V} + \mathrm{Pr}(RaT - Rn\varphi)\mathbf{e_z} + \frac{\mathrm{Pr}^2Q}{\mathrm{Pr}_M}(\nabla \times \mathbf{H}) \times \mathbf{H}, \tag{15}$$

$$\frac{\partial T}{\partial t}+(\mathbf{V}.\nabla)T=\nabla^2 T+\frac{N_A N_B}{Le}\nabla T.\nabla T+\frac{N_B}{Le}\nabla\varphi.\nabla T-N_B\varphi\mathbf{V}.\nabla T, \tag{16}$$

$$\frac{\partial \varphi}{\partial t}+(\mathbf{V}.\nabla)\varphi=\frac{N_A}{Le}\nabla^2 T+\frac{1}{Le}\nabla^2\varphi, \tag{17}$$

$$\nabla.\mathbf{H}=0, \tag{18}$$

$$\frac{\partial \mathbf{H}}{\partial t}+(\mathbf{V}.\nabla)\mathbf{H}=(\mathbf{H}.\nabla)\mathbf{V}+\frac{\mathrm{Pr}}{\mathrm{Pr}_M}\nabla^2\mathbf{H}. \tag{19}$$

Accordingly, the corresponding non-dimensional boundary conditions are expressed as:

$$\begin{cases} w=Pe,\ \dfrac{\partial w}{\partial z}=0,\ N_A\dfrac{\partial T}{\partial z}+\dfrac{\partial \varphi}{\partial z}-PeLe\,\varphi=0,\ T=1,\ H_z=1,\ \dfrac{\partial H_z}{\partial z}=0\ \text{ at }\ z=0, \\ w=Pe,\ \dfrac{\partial w}{\partial z}=0,\ N_A\dfrac{\partial T}{\partial z}+\dfrac{\partial \varphi}{\partial z}-PeLe\,\varphi=0,\ T=0,\ H_z=1,\ \dfrac{\partial H_z}{\partial z}=0\ \text{ at }\ z=1. \end{cases} \tag{20}$$

It is worth pointing out that the physical meanings of the non-dimensional parameters shown in Eqs. (15)–(19) as well as their explicit expressions are enlisted clearly in Table 1. In this tabular representation, the dynamical microscopic quantities D_B and D_T explore the Brownian and Thermophoresis diffusion coefficients, respectively. Also, it is more practical to discuss the stability of the problem via the control parameters Nb and Nt instead of considering the modified parameters $N_B(=NbLe)$ and $N_A(=Nt/Nb)$.

2.2. Basic state

The basic state of the present stability problem is assumed to be quiescent (i.e., $\partial/\partial t=0$) with the z-spatial dependence, whose physical characteristics are written as:

$$\mathbf{V_b}=Pe\,\mathbf{e_z},\ P_b=P_b(z),\ T_b=T_b(z),\ \varphi_b=\varphi_b(z),\ \mathbf{H_b}=H_b(z)\mathbf{e_z}. \tag{21}$$

After substituting Eq. (21) into Eqs.(15)–(19), we get:

$$\nabla[P_b(z)+\mathrm{Pr}(R_M+Ra)z]=\mathrm{Pr}(RaT_b(z)-Rn\varphi_b(z))\mathbf{e_z}+\frac{\mathrm{Pr}^2 Q}{\mathrm{Pr}_M}(\nabla\times\mathbf{H_b}(z))\times\mathbf{H_b}(z), \tag{22}$$

$$Pe\frac{dT_b(z)}{dz}=\frac{d^2T_b(z)}{dz^2}+\frac{N_B}{Le}\left(N_A\frac{dT_b(z)}{dz}+\frac{d\varphi_b(z)}{dz}-PeLe\varphi_b(z)\right)\frac{dT_b}{dz}, \tag{23}$$

$$\frac{d}{dz}\left(N_A\frac{dT_b(z)}{dz}+\frac{d\varphi_b(z)}{dz}-PeLe\,\varphi_b(z)\right)=0, \tag{24}$$

Table 1
Physical meanings and expressions of the embedded physical parameters.

Physical parameters	Symbols	Expressions
Density Rayleigh number	R_M	$\frac{[\rho_0(1-\varphi_0)+\rho_S\varphi_0]gL^3}{\mu\alpha}$
Thermal Rayleigh number	Ra	$\frac{\rho_0\beta(T_H-T_C)gL^3}{\mu\alpha}$
Nanoparticle Rayleigh number	Rn	$\frac{(\rho_S-\rho_0)gL^3\varphi_0}{\mu\alpha}$
Magnetic Chandrasekhar number	Q	$\frac{\mu_e H_0^2 L^2}{4\pi\mu\eta}$
Prandtl number	Pr	$\frac{\mu}{\rho_0\alpha}$
Magnetic Prandtl number	Pr_M	$\frac{\mu}{\rho_0\eta}$
Modified specific heat increment	N_B	$\frac{(\rho C_P)_S\varphi_0}{(\rho C_P)}$
Brownian motion parameter	Nb	$\frac{(\rho C_P)_S D_B\varphi_0}{(\rho C_P)\alpha}$
Lewis number	Le	$\frac{\alpha}{D_B}$
Modified diffusivity ratio	N_A	$\frac{D_T(T_H-T_C)}{D_B\varphi_0 T_H}$
Thermophoresis parameter	Nt	$\frac{D_T(\rho C_P)_S(T_H-T_C)}{\alpha(\rho C_P)T_H}$
Péclet number	Pe	$\frac{Lw_0}{\alpha}$

$$Pe\frac{dH_b(z)}{dz} = \frac{\Pr}{\Pr_M}\frac{d^2H_b(z)}{dz^2}, \tag{25}$$

$$\frac{dH_b(z)}{dz} = 0. \tag{26}$$

Once more, these ordinary differential equations are managed by the following boundary conditions:

$$\begin{cases} N_A\frac{dT_b}{dz} + \frac{d\varphi_b}{dz} - PeLe\,\varphi_b = 0,\ T_b = 1,\ H_b = 1 \ \text{ at } \ z = 0, \\ N_A\frac{dT_b}{dz} + \frac{d\varphi_b}{dz} - PeLe\,\varphi_b = 0,\ T_b = 0,\ H_b = 1 \ \text{ at } \ z = 1, \end{cases} \tag{27}$$

The preliminary mathematical integrations of Eqs. (24)–(26) along with the above boundary conditions yield to the following results:

$$\frac{d\varphi_b(z)}{dz} - PeLe\,\varphi_b(z) = -N_A\frac{dT_b(z)}{dz}, \tag{28}$$

$$H_b(z) = 1. \tag{29}$$

By making use of Eq. (28) in Eq. (23), we obtain:

$$\frac{d^2T_b(z)}{dz^2} = Pe\frac{dT_b(z)}{dz}. \tag{30}$$

This linear thermal differential equation has the following closed-form solution:

$$T_b(z) = \frac{exp(Pe) - exp(Pez)}{exp(Pe) - 1}. \tag{31}$$

By adopting Wakif's conservative law [29], we can write:

$$\frac{1}{L}\int_0^L \varphi_b^*(z^*)dz^* = \varphi_0 \quad \left(\text{i.e., } \int_0^1 \varphi_b(z)dz = 0\right) \tag{32}$$

Based on Eqs. (31) and (32), the following exact solution can be derived for Eq (28):

$$\varphi_b(z) = \left(\frac{N_A Le}{Le - 1}\right)\left[\frac{exp(PeLez)}{exp(PeLe) - 1} - \frac{exp(Pez)}{Le(exp(Pe) - 1)}\right] \tag{33}$$

In the nonexistence of the blowing/suction effect (i.e., $Pe = 0$), the thermal and mass basic solutions exhibit a linear variation concerning the spatial variable z. In this limiting case, these special solutions take the following forms:

$$\overline{T}_b(z) = \lim_{Pe\to 0} T_b(z) = 1 - z, \tag{34}$$

$$\overline{\varphi}_b(z) = \lim_{Pe\to 0} \varphi_b(z) = N_A\left(z - \frac{1}{2}\right) \tag{35}$$

An interesting affirmation can be exclusively stated here for the analytical expressions given by Eqs. (34) and (35) is that the analytical expressions of the basic solutions $T_b(z)$ and $\varphi_b(z)$ are coincided exactly with the Wakif's results pointed out previously in Refs. [28,29,31,32].

2.3. Perturbed state

The thermal stability of the present basic nanofluid flow model can be examined properly by utilizing the linear stability theory. For this purpose, the basic state of the nanofluidic medium $(\mathbf{V_b}, T_b, P_b, \varphi_b, \mathbf{H_b})$ can be disturbed via an infinitesimal thermal perturbation T' to produce further slight perturbations $\mathbf{V}'$, P', φ' and $\mathbf{H}'$ for the other basic quantities $\mathbf{V_b}$, P_b, φ_b and $\mathbf{H_b}$, respectively. As a result, the desired dimensionless solutions are sought to be in the following specific forms:

$$\mathbf{V} = \mathbf{V_b} + \mathbf{V}', \quad T = T_b + T', \quad P = P_b + P', \quad \varphi = \varphi_b + \varphi', \quad \mathbf{H} = \mathbf{H_b} + \mathbf{H}'. \tag{36}$$

After inserting Eq. (36) into Eqs. (14)–(19) and linearizing the resulting equations, we end up with the following linear perturbation equations:

$$\nabla.\mathbf{V}' = 0, \tag{37}$$

$$\frac{\partial \mathbf{V}^{'}}{\partial t} = -\nabla P^{'} + \mathrm{Pr}\nabla^2 \mathbf{V}^{'} - Pe\frac{\partial \mathbf{V}^{'}}{\partial z} + \mathrm{Pr}(RaT^{'} - Rn\varphi^{'})\mathbf{e_z} + \frac{\mathrm{Pr}^2 Q}{\mathrm{Pr}_M}(\nabla \times \mathbf{H}^{'}) \times \mathbf{e_z}, \tag{38}$$

$$\frac{\partial T^{'}}{\partial t} = -\frac{dT_b}{dz}(1 + N_B\varphi_b)w^{'} + \nabla^2 T^{'} + \left(\frac{N_A N_B}{Le}\frac{dT_b}{dz} - Pe\right)\frac{\partial T^{'}}{\partial z} + N_B\frac{dT_b}{dz}\left(\frac{1}{Le}\frac{\partial \varphi^{'}}{\partial z} - Pe\,\varphi^{'}\right), \tag{39}$$

$$\frac{\partial \varphi^{'}}{\partial t} = -\frac{d\varphi_b}{dz}w^{'} + \frac{N_A}{Le}\nabla^2 T^{'} + \frac{1}{Le}\nabla^2\varphi^{'} - Pe\frac{\partial \varphi^{'}}{\partial z}, \tag{40}$$

$$\nabla.\mathbf{H}^{'} = 0, \tag{41}$$

$$\frac{\partial \mathbf{H}^{'}}{\partial t} = \frac{\partial \mathbf{V}^{'}}{\partial z} + \frac{\mathrm{Pr}}{\mathrm{Pr}_M}\nabla^2 \mathbf{H}^{'} - Pe\frac{\partial \mathbf{H}^{'}}{\partial z}. \tag{42}$$

To eliminate the pressure gradient term from Eq. (38), we have applied successively the curl operator twice to this equation along with Eqs. (37) and (41). In this situation, the z-component of the ensuing equation is written as:

$$\frac{\partial}{\partial t}\left(\nabla^2 w^{'}\right) = \mathrm{Pr}\nabla^4 w^{'} - Pe\frac{\partial}{\partial z}\left(\nabla^2 w^{'}\right) + \mathrm{Pr}\left(Ra\nabla_H^2 T^{'} - Rn\nabla_H^2\varphi^{'}\right) + \frac{\mathrm{Pr}^2 Q}{\mathrm{Pr}_M}\frac{\partial}{\partial z}\left(\nabla^2 H_z^{'}\right) \tag{43}$$

Here, $\nabla_H^2\left(=\partial^2/\partial x^2 + \partial^2/\partial y^2\right)$ is the horizontal Laplacian operator.

Additionally, the z-component of Eq. (42) takes the following form:

$$\frac{\partial H_z^{'}}{\partial t} = \frac{\partial w^{'}}{\partial z} + \frac{\mathrm{Pr}}{\mathrm{Pr}_M}\nabla^2 H_z^{'} - Pe\frac{\partial H_z^{'}}{\partial z}. \tag{44}$$

2.4. Normal mode analysis

The temporal and spatial characteristics of the aforementioned perturbations $\left(w^{'}, T^{'}, \varphi^{'}, H_z^{'}\right)$ are scrutinized appropriately by regarding them physically as periodic waves, whose analytical expressions are given by:

$$\begin{cases} w^{'}(x,y,z,t) = W(z)exp\left[i\left(a_x x + a_y y\right) + \lambda t\right], \\ T^{'}(x,y,z,t) = \theta(z)exp\left[i\left(a_x x + a_y y\right) + \lambda t\right], \\ \varphi^{'}(x,y,z,t) = \Phi(z)exp\left[i\left(a_x x + a_y y\right) + \lambda t\right], \\ H_z^{'}(x,y,z,t) = \tau(z)exp\left[i\left(a_x x + a_y y\right) + \lambda t\right], \end{cases} \tag{45}$$

where λ is the growth rate of the disturbances and (a_x, a_y) are the wave-number components in the x- and y- directions, respectively.

After substituting Eq. (45) into Eqs. (39), (40), (43) and (44), we get

$$\left[\mathrm{Pr}\left(D^{(2)} - a^2\right) - PeD - \lambda\right]\left(D^{(2)} - a^2\right)W - \mathrm{Pr}Ra\,a^2\theta + \mathrm{Pr}Rn\,a^2\Phi + \frac{\mathrm{Pr}^2 Q}{\mathrm{Pr}_M}D\left(D^{(2)} - a^2\right)\tau = 0, \tag{46}$$

$$-\frac{dT_b}{dz}(1 + N_B\varphi_b)W + \left[\left(D^{(2)} - a^2\right) + \left(\frac{N_A N_B}{Le}\frac{dT_b}{dz} - Pe\right)D - \lambda\right]\theta + N_B\frac{dT_b}{dz}\left(\frac{1}{Le}D - Pe\right)\Phi = 0, \tag{47}$$

$$-\frac{d\varphi_b}{dz}W + \frac{N_A}{Le}\left(D^{(2)} - a^2\right)\theta + \left[\frac{1}{Le}\left(D^{(2)} - a^2\right) - Pe\,D - \lambda\right]\Phi = 0, \tag{48}$$

$$DW + \left[\frac{\mathrm{Pr}}{\mathrm{Pr}_M}\left(D^{(2)} - a^2\right) - Pe\,D - \lambda\right]\tau = 0. \tag{49}$$

Here, $D^{(n)} \equiv d^n/\mathrm{d}z^n$ and $a^2 = a_x^2 + a_y^2$, where n is an integer derivative order and $D \equiv \mathrm{d}/\mathrm{d}z$.

The system of Eqs. (46)–(49) is controlled by the following boundary conditions:

$$W = DW = \theta = N_A D\theta + D\Phi - PeLe\,\Phi = D\tau = 0 \ \text{ at } \ z = 0, 1. \tag{50}$$

3. Method of solution

As proved before, the governing stability equations (46)–(49) together with their appropriate boundary conditions (50) constitute a linear eigenvalue problem of finite dimension, whose eigenvalues are selected to be the possible values of the thermal Rayleigh number Ra. This eigenvalue problem can be solved numerically via the Chebyshev-Gauss-Lobatto Spectral Method (CGLSM) [25,35,36]. To apply correctly this innovative numerical procedure, it is recommended to consider a novel spatial variable ξ, which is defined as:

$$\begin{cases} z = \dfrac{1}{2}(\xi + 1) \ \text{ where } \ 0 \le z \le 1 \ \text{ and } \ -1 \le \xi \le 1, \\ D^{(n)} = 2^n \overline{D}^{(n)} \ \text{ where } \ \overline{D}^{(n)} = \dfrac{d^n}{d\xi^n}. \end{cases} \tag{51}$$

By assuming that the principle of exchange of thermal stability holds for the present nanofluid stability problem, the occurred stationary convection mode can be evidenced compressively by introducing the following nanoparticles mass flux unknown:

$$\Gamma = -(N_A D\theta + D\Phi - PeLe\, \Phi) \tag{52}$$

For further computational simplifications, the final unknown functions $(W, \theta, \Gamma, \tau)$ together with the basic solutions (T_b, φ_b) are subjected to the following spatial transformations:

$$\begin{cases} W(z) = W\left(\dfrac{1}{2}\xi + \dfrac{1}{2}\right) = \overline{W}(\xi), \\ \theta(z) = \theta\left(\dfrac{1}{2}\xi + \dfrac{1}{2}\right) = \overline{\theta}(\xi), \\ \Gamma(z) = \Gamma\left(\dfrac{1}{2}\xi + \dfrac{1}{2}\right) = \overline{\Gamma}(\xi), \\ \tau(z) = \tau\left(\dfrac{1}{2}\xi + \dfrac{1}{2}\right) = \overline{\tau}(\xi), \\ T_b(z) = T_b\left(\dfrac{1}{2}\xi + \dfrac{1}{2}\right) = \overline{T}_b(\xi), \\ \varphi_b(z) = \varphi_b\left(\dfrac{1}{2}\xi + \dfrac{1}{2}\right) = \overline{\varphi}_b(\xi) \end{cases} \tag{53}$$

Therefore, the stationary forms of Eqs. (46)-(49) can be rearranged as:

$$A_{\overline{W}}\overline{W} + A_{\overline{\theta}}\overline{\theta} + A_{\overline{\Gamma}}\overline{\Gamma} + A_{\overline{\tau}}\overline{\tau} = Ra\, E_{\overline{\theta}}\overline{\theta}, \tag{54}$$

$$B_{\overline{W}}\overline{W} + B_{\overline{\theta}}\overline{\theta} + B_{\overline{\Gamma}}\overline{\Gamma} = 0, \tag{55}$$

$$C_{\overline{W}}\overline{W} + C_{\overline{\theta}}\overline{\theta} + C_{\overline{\Gamma}}\overline{\Gamma} = 0, \tag{56}$$

$$D_{\overline{W}}\overline{W} + D_{\overline{\tau}}\overline{\tau} = 0, \tag{57}$$

where

$$\overline{W} = \overline{DW} = \overline{\theta} \ = \overline{\Gamma} = \overline{D\tau} = 0 \ \text{ at } \ \xi = -1, 1. \tag{58}$$

It bears noting that the differential operators $\left(A_{\overline{W}}, A_{\overline{\theta}}, A_{\overline{\Gamma}}, A_{\overline{\tau}}, B_{\overline{W}}, B_{\overline{\theta}}, B_{\overline{\Gamma}}, C_{\overline{W}}, C_{\overline{\theta}}, C_{\overline{\Gamma}}, D_{\overline{W}}, D_{\overline{\tau}}, E_{\overline{\theta}}\right)$ used in Eqs. (54)–(57) are

Table 2
Expressions of the embedded differential operators.

Differential operators	Expressions
$A_{\overline{W}}$	$16\overline{D}^{(4)} - \dfrac{8Pe}{\mathrm{Pr}}\overline{D}^{(3)} - 8a^2\overline{D}^{(2)} + \dfrac{2Pe\, a^2}{\mathrm{Pr}}\overline{D} + a^4 - 2RnLe\left(\overline{D}\overline{\varphi}_b\right)$
$A_{\overline{\theta}}$	$-RnN_A a^2$
$A_{\overline{\Gamma}}$	$-2Rn\overline{D}$
$A_{\overline{\tau}}$	$\dfrac{2\mathrm{Pr}Q}{\mathrm{Pr}_M}(4\overline{D}^{(3)} - a^2\overline{D})$
$B_{\overline{W}}$	$2(\overline{D}\overline{T}_b)(1 + N_B\overline{\varphi}_b)$
$B_{\overline{\theta}}$	$-4\overline{D}^{(2)} + 2Pe\,\overline{D} + a^2$
$B_{\overline{\Gamma}}$	$\dfrac{2N_B}{Le}\left(\overline{D}\overline{T}_b\right)$
$C_{\overline{W}}$	$4(\overline{D}\overline{\varphi}_b)\overline{D} - 4N_A(\overline{D}^{(2)}\overline{T}_b)$
$C_{\overline{\theta}}$	$-PeN_A a^2$
$C_{\overline{\Gamma}}$	$\dfrac{1}{Le}\left(4\overline{D}^{(2)} - 2PeLe\,\overline{D} - a^2\right)$
$D_{\overline{W}}$	$2\overline{D}$
$D_{\overline{\tau}}$	$\dfrac{4\mathrm{Pr}}{\mathrm{Pr}_M}\overline{D}^{(2)} - 2Pe\,\overline{D} - \dfrac{\mathrm{Pr}a^2}{\mathrm{Pr}_M}$
$E_{\overline{\theta}}$	a^2

summarized in Table 2. Additionally, these equations can be assembled in the matrix form as follows:

$$\begin{pmatrix} A_{\overline{W}} & A_{\overline{\theta}} & A_{\overline{\Gamma}} & A_{\overline{\tau}} \\ B_{\overline{W}} & B_{\overline{\theta}} & B_{\overline{\Gamma}} & 0 \\ C_{\overline{W}} & C_{\overline{\theta}} & C_{\overline{\Gamma}} & 0 \\ D_{\overline{W}} & 0 & 0 & D_{\overline{\tau}} \end{pmatrix} \begin{pmatrix} \overline{W} \\ \overline{\theta} \\ \overline{\Gamma} \\ \overline{\tau} \end{pmatrix} = Ra \begin{pmatrix} 0 & E_{\overline{\theta}} & 0 & 0 \\ 0 & 0 & 0 & 0 \\ 0 & 0 & 0 & 0 \\ 0 & 0 & 0 & 0 \end{pmatrix} \begin{pmatrix} \overline{W} \\ \overline{\theta} \\ \overline{\Gamma} \\ \overline{\tau} \end{pmatrix} \tag{59}$$

The linear eigenvalue problem described by Eq. (59) is discretized spatially using CGLSM along with the Gauss - Lobatto Collocation Grid Points (GLCGPs), which are defined as [37–41]:

$$\xi_i = cos\left(\frac{\pi i - \pi}{N-1}\right), \tag{60}$$

where $1 \le i \le N$ and $\xi_N \le \xi_i \le \xi_1$.

Further, the first-order derivative matrix $D = \left(\left(\tilde{d}_{ij}\right)_{1\le i,j\le N}\right)$ and its corresponding n^{th}- order derivative $D^{(n)} = \left(\left(\tilde{d}_{ij}^{(n)}\right)_{1\le i,j\le N}\right)$ are given by Canuto et al. [42] and Trefethen [43] as:

$$\begin{cases} \tilde{d}_{ij} = \dfrac{2(N-1)^2+1}{6} \text{ when } i=j=1, \\ \tilde{d}_{ij} = -\dfrac{\xi_i}{2\left(1-\xi_i^2\right)} \text{ when } i=j\neq 1,N, \\ \tilde{d}_{ij} = \dfrac{(-1)^{i+j}C_i}{C_j\left(\xi_i-\xi_j\right)} \text{ when } i\neq j, \\ \tilde{d}_{ij} = -\dfrac{2(N-1)^2+1}{6} \text{when } i=j=N, \end{cases} \tag{61}$$

$$\begin{cases} C_i = 2 \quad \text{for } i = 1,N, \\ C_i = 1 \quad \text{for } i \neq 1,N, \end{cases} \tag{62}$$

$$\tilde{d}_{ij}^{(n)} = \sum_{k=1}^{N}\left(\tilde{d}_{ik}^{(n-1)}\tilde{d}_{kj}\right) \tag{63}$$

Based on the numerical procedure CGLSM, the derivative terms appeared in Eqs. (54)–(57) and defined in Table 2 can be

Table 3
Expressions of the used matrix elements.

Matrix elements	Expressions
$(A_{\overline{W}})_{ij}$	$16\tilde{D}_{ij}^{(4)} - \frac{8Pe}{\mathrm{Pr}}\tilde{D}_{ij}^{(3)} - 8a^2\tilde{D}_{ij}^{(2)} + \frac{2Pe\,a^2}{\mathrm{Pr}}\tilde{D}_{ij} + \left[a^4 - 2RnLe\left(\overline{D}\overline{\varphi}_b\right)_i\right]\delta_{ij}$
$(A_{\overline{\theta}})_{ij}$	$-RnN_Aa^2\delta_{ij}$
$(A_{\overline{\Gamma}})_{ij}$	$-2Rn\tilde{d}_{ij}$
$(A_{\overline{\tau}})_{ij}$	$\frac{2\mathrm{Pr}Q}{\mathrm{Pr}_M}(4\tilde{\tilde{D}}_{ij}^{(3)} - a^2\tilde{\tilde{D}}_{ij})$
$(B_{\overline{W}})_{ij}$	$2\left(\overline{DT}_b\right)_i\left[1+N_B\left(\overline{\varphi}_b\right)_i\right]\delta_{ij}$
$(B_{\overline{\theta}})_{ij}$	$-4\tilde{d}_{ij}^{(2)} + 2Pe\,\tilde{d}_{ij} + a^2\delta_{ij}$
$(B_{\overline{\Gamma}})_{ij}$	$\frac{2N_B}{Le}\left(\overline{DT}_b\right)_i\delta_{ij}$
$(C_{\overline{W}})_{ij}$	$4\left(\overline{D}\overline{\varphi}_b\right)_i\tilde{D}_{ij} - 4N_A\left(\overline{D}^{(2)}\overline{T}_b\right)_i\delta_{ij}$
$(C_{\overline{\theta}})_{ij}$	$-PeN_Aa^2\delta_{ij}$
$(C_{\overline{\Gamma}})_{ij}$	$\frac{1}{Le}\left(4\tilde{d}_{ij}^{(2)} - 2PeLe\,\tilde{d}_{ij} - a^2\delta_{ij}\right)$
$(D_{\overline{W}})_{ij}$	$2\tilde{D}_{ij}$
$(D_{\overline{\tau}})_{ij}$	$\frac{4\mathrm{Pr}}{\mathrm{Pr}_M}\tilde{\tilde{D}}_{ij}^{(2)} - 2Pe\tilde{\tilde{D}}_{ij} - \frac{\mathrm{Pr}a^2}{\mathrm{Pr}_M}\delta_{ij}$
$(E_{\overline{\theta}})_{ij}$	$a^2\delta_{ij}$
Z_{ij}	0

approximated locally as follows:

$$\begin{cases} \overline{D}^{(n)}\overline{W}(\xi_i) = \sum_{j=1}^{N} \tilde{d}_{ij}^{(n)}\overline{W}(\xi_j),\ \overline{D}^{(n)}\overline{\theta}(\xi_i) = \sum_{j=1}^{N} \tilde{d}_{ij}^{(n)}\overline{\theta}(\xi_j), \\ \overline{D}^{(n)}\overline{\Gamma}(\xi_i) = \sum_{j=1}^{N} \tilde{d}_{ij}^{(n)}\overline{\Gamma}(\xi_j),\ \overline{D}^{(n)}\overline{\tau}(\xi_i) = \sum_{j=1}^{N} \tilde{d}_{ij}^{(n)}\overline{\tau}(\xi_j), \end{cases} \tag{64}$$

where $1 \le i \le N$ and $-1 \le \xi_i \le 1$.

By making use of Eqs. (58)–(64), the following discretized eigenvalue problem is derived:

$$\begin{pmatrix} (A_{\overline{W}})_{ij} & (A_{\overline{\theta}})_{ij} & (A_{\overline{\Gamma}})_{ij} & (A_{\overline{\tau}})_{ij} \\ (B_{\overline{W}})_{ij} & (B_{\overline{\theta}})_{ij} & (B_{\overline{\Gamma}})_{ij} & Z_{ij} \\ (C_{\overline{W}})_{ij} & (C_{\overline{\theta}})_{ij} & (C_{\overline{\Gamma}})_{ij} & Z_{ij} \\ (D_{\overline{W}})_{ij} & Z_{ij} & Z_{ij} & (D_{\overline{\tau}})_{ij} \end{pmatrix}_{2\le i,j\le N-1} \begin{pmatrix} \overline{W}_j \\ \overline{\theta}_j \\ \overline{\Gamma}_j \\ \overline{\tau}_j \end{pmatrix} = Ra \begin{pmatrix} Z_{ij} & (E_{\overline{\theta}})_{ij} & Z_{ij} & Z_{ij} \\ Z_{ij} & Z_{ij} & Z_{ij} & Z_{ij} \\ Z_{ij} & Z_{ij} & Z_{ij} & Z_{ij} \\ Z_{ij} & Z_{ij} & Z_{ij} & Z_{ij} \end{pmatrix}_{2\le i,j\le N-1} \begin{pmatrix} \overline{W}_j \\ \overline{\theta}_j \\ \overline{\Gamma}_j \\ \overline{\tau}_j \end{pmatrix} \tag{65}$$

For more clarifications, the above system is built properly in such a way that the final form of the boundary conditions (i.e., Eq. (58)) are introduced implicitly in the matrix elements of the eigenvalue problem described by Eq. (65). These modified elements are defined tabularly as shown in Table 3 and Table 4.

The mathematical element δ_{ij} shown in Table 3 and Table 4 defines the Kronecker symbol, which is given by:

$$\begin{cases} \delta_{ij} = 0 & \text{if } i \ne j, \\ \delta_{ij} = 1 & \text{if } i = j. \end{cases} \tag{66}$$

The generalized linear eigenvalue problem described by Eq. (65) can be also written as:

$$\mathbf{M}\,\mathbf{X} = Ra\,\mathbf{M}^{'}\,\mathbf{X}. \tag{67}$$

Here, $\mathbf{M}$ and $\mathbf{M}^{'}$ represent two $(4N-8)\times(4N-8)$ square matrices, Ra shows the generalized eigenvalues and $\mathbf{X}$ stands for the unknown vector column of the present stability problem.

By using the predefined "eig" Matlab function, the real eigenvalue Ra is determined when the other control parameters are specified. For this purpose, the wave-number a can be fixed to determine the $(4N-8)$ eigenvalues Ra_i of the system (67). Among these $(4N-8)$ eigenvalues, only $N^{'}$ positive real eigenvalues can be retained physically (i.e., $N^{'} < 4N-8$). Furthermore, the thermal Rayleigh number Ra sought for the wave-number a is computed as follows:

$$Ra(a) = min(\{Ra_i,\ \text{where } 1 \le i \le 4N-8\}) \tag{68}$$

Accordingly, an eigenvalue spectrum $S_a = \{Ra(a_i), \text{where } a_1 \le a_i \le a_2\}$ is constructed for specified ranging values of the wave-number a(i.e., $a_i \le a \le a_f$). Based on this set of eigenvalues, the neutral stability curve $Ra = f(a)$ of the stationary convective mode can be portrayed accordingly. In this regards, the critical point (a_C, Ra_C) featured the thermal stability of the nanofluidic medium is defined as:

$$Ra_C = min(S_a), \tag{69}$$

Table 4
Expressions of the modified matrix elements.

Modified matrix elements	Expressions
$\tilde{D}_{ij}$	$\frac{1}{(1-\xi_i^2)}[(1-\xi_i^2)\tilde{d}_{ij} - 2\xi_i\delta_{ij}]$
$\tilde{D}_{ij}^{(2)}$	$\frac{1}{(1-\xi_i^2)}[(1-\xi_i^2)\tilde{d}_{ij}^{(2)} - 4\xi_i\tilde{d}_{ij} - 2\delta_{ij}]$
$\tilde{D}_{ij}^{(3)}$	$\frac{1}{(1-\xi_i^2)}[(1-\xi_i^2)\tilde{d}_{ij}^{(3)} - 6\xi_i\tilde{d}_{ij}^{(2)} - 6\tilde{d}_{ij}]$
$\tilde{D}_{ij}^{(4)}$	$\frac{1}{(1-\xi_i^2)}[(1-\xi_i^2)\tilde{d}_{ij}^{(4)} - 8\xi_i\tilde{d}_{ij}^{(3)} - 12\tilde{d}_{ij}^{(2)}]$
$\tilde{\tilde{D}}_{ij}$	$\tilde{d}_{ij} + \tilde{d}_{i1}\alpha_j + \tilde{d}_{iN}\beta_j$
$\tilde{\tilde{D}}_{ij}^{(2)}$	$\tilde{d}_{ij}^{(2)} + \tilde{d}_{i1}^{(2)}\alpha_j + \tilde{d}_{iN}^{(2)}\beta_j$
$\tilde{\tilde{D}}_{ij}^{(3)}$	$\tilde{d}_{ij}^{(3)} + \tilde{d}_{i1}^{(3)}\alpha_j + \tilde{d}_{iN}^{(3)}\beta_j$
α_j	$\frac{\tilde{d}_{1N}\tilde{d}_{Nj} - \tilde{d}_{NN}\tilde{d}_{1j}}{\tilde{d}_{11}\tilde{d}_{NN} - \tilde{d}_{1N}\tilde{d}_{N1}}$
β_j	$\frac{\tilde{d}_{N1}\tilde{d}_{1j} - \tilde{d}_{11}\tilde{d}_{Nj}}{\tilde{d}_{11}\tilde{d}_{NN} - \tilde{d}_{1N}\tilde{d}_{N1}}$

$$Ra_C = Ra(a_C) \tag{70}$$

Additionally, the optimum values of the critical stability parameters (Ra_C, a_C) depend strongly on the physical parameters involved therein, which are highlighted symbolically by $Rn, Pe, Q, N_B, N_A, \mathrm{Pr}, \mathrm{Pr}_M$ and Le. For the monotypic nanofluids $Al_2O_3 - H_2O$ conveying tiny-sized alumina nanomaterials, whose spherical diameter d_S and volume fraction φ_0 are taken respectively in the range of 30nm − 45nm and 1% − 4%, the values of the nanofluid parameters $Rn, Nb, Nt, N_B, N_A, \mathrm{Pr}, \mathrm{Pr}_M$ and Le are computed previously by wakif et al. [31]. These magnitudes can briefly be summed up as follows:

$$Rn \sim 10^{-1} - 10^{0}, (Nb, Nt) \sim \left(10^{-6}, 10^{-6}\right), (N_B, N_A) \sim \left(10^{-2}, 10^{0}\right), (\mathrm{Pr}, \mathrm{Pr}_M) \sim \left(10^{1}, 10^{-12}\right), Le \sim 10^{4}. \tag{71}$$

Moreover, in another related work, wakif et al. [32] proved that the Lewis number Le for the hybrid nanofluids $(Al_2O_3 + CuO) - H_2O$ can be estimated in the order of 10^3, when $\varphi_{Al_2O_3} = \varphi_{CuO}$, $d_S = d_{Al_2O_3} = d_{CuO}$ and $d_S < 20nm$. Keeping in mind that the main characteristic parameters Nb,Nt and Pr_M exhibit nearly lesser degrees of variability towards the growing values of the nanoparticles volume fraction φ_0 introduced initially in the base fluid. So, it is more practical to control the thermal stability of the nanofluidic medium only through the main embedded parameters Rn, Pe, Q and Le.

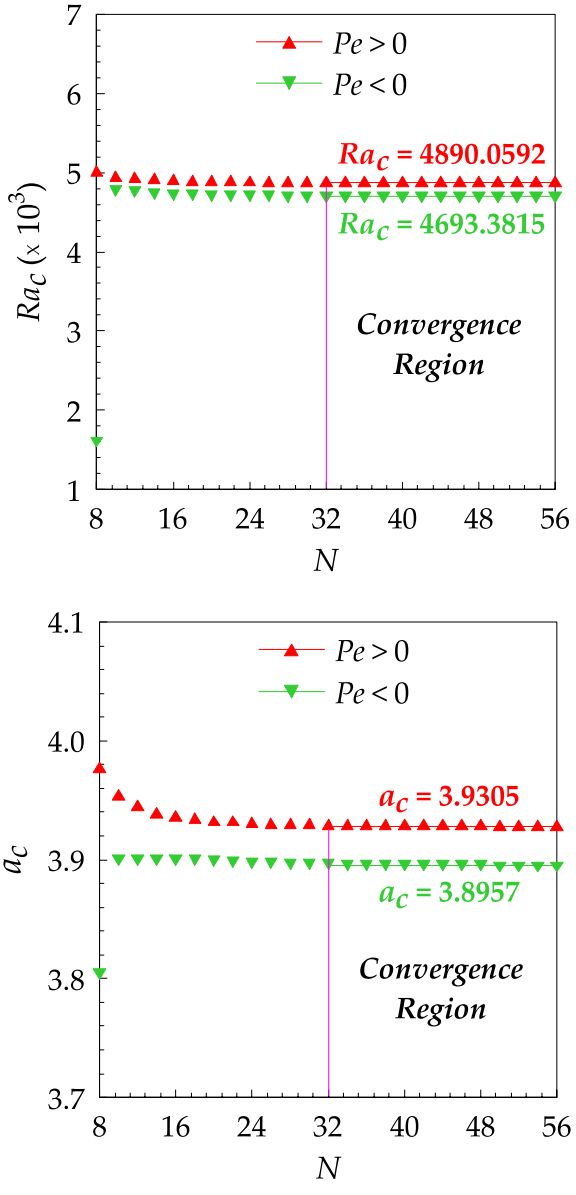

Fig. 2. Convergence of CGLSM results in terms of the stability parameters (Ra_C, a_C).

4. Results and discussion

As mentioned previously, the thermal stability of the studied nanofluidic layer depends ostensibly on eight parameters (i.e., $Rn, Pe, Q, N_B, N_A, \mathrm{Pr}, \mathrm{Pr}_M$ and Le) By taking into account the previously discussed restrictions, the concerned control parameters are reduced only to the most significant ones, which are Rn,Pe,Q and Le. In this regards, the parameter values $Rn = 0.3$, $|Pe| = 0.01$, $Q = 10$, $\mathrm{Pr} = 7$ and $Le = 1000$ are designated as tentative inputs that are required to optimize the critical values (Ra_C, a_C) controlling the thermal stability of the nanofluidic medium, which are selected as default parameter values unless otherwise indicated herein (i.e., graphically or tabularly). These concerned physical parameters are adjusted accordingly during the numerical simulation to reflect the behavior of each parameter on the appearance of nanofluid convection in the confined medium. However, the parameters $\mathrm{Pr}, \mathrm{Pr}_M, N_B$ and N_A have been kept unchanged in the whole analysis, where $\mathrm{Pr} = 7$, $\mathrm{Pr}_M = 10^{-12}$, $N_B = 10^{-2}$ and $N_A = 1$. Furthermore, the stationary neutral stability curves and their corresponding stability parameters (Ra_C, a_C) portrayed in Figs. 6–9 and Tables 7–10 are generated properly by choosing $N = 32$ as the total number of GLCGPs and ranging the wave-number a by a fixed step-size of about $\Delta a = 0.0001$ to achieve a higher level of absolute accuracy, which is estimated to be of the order of 10^{-4} as proved in Fig. 2.

From an efficiency point of view, the robustness and validity of the proposed CGLSM numerical scheme are justified tabularly by carrying out various comparative attempts as quantified numerically in Table 5 and Table 6 between the present numerical results and those established previously for some limiting cases (i.e., $\varphi_0 = 0$ and $Pe = 0$) with the help of other powerful computational methods, like Chandrasekhar's Variational Method (CVM) [44], Runge-Kutta-Fehlberg Method (RKFM) [30], Power Series Method (PSM) [32], Generalized Differential Quadrature Method (GDQM) [31] and Wakif-Galerkin Weighted Residuals Technique (WGWRT) [31]. A quantitative evaluation of the results of Table 5 and Table 6 indicates that there is an excellent degree of harmony between the CGLSM results and those of the existing literature survey. Hence, the validity of the proposed method together with the exactness of the obtained results are confirmed reasonably.

On the other hand, to reveal the thermal and mass features of the basic nanofluid flow against the varying values of the involved flow parameters Pe and Le, Eqs. (31) and (33)–(35) are exploited appropriately to plot the basic profiles $T_b(z)$ and $\varphi_b(z)$ as exposed in Figs. 3–5. From Fig. 3, it is remarked that the amplifying blowing effect (i.e., $Pe > 0$) has an enhancing trend on the basic temperature throughout the nanofluidic medium. However, a noticeable dissimilar tendency is perceived for the suction case (i.e., $Pe < 0$) Other obvious disturbance influences of the wall blowing/suction velocity (i.e., $Pe \neq 0$) are demonstrated perfectly via the profiles of $\varphi_b(z)$ in Fig. 4 for the spatial distribution of nanoparticles inside the medium, in which $\varphi_b(z \to 0) < 0$ and $\varphi_b(z \to 1) > 0$. In this display, it is found that the blowing effect (i.e., $Pe > 0$) produces a notable top-heavy distribution of nanoparticles near the upper permeable plate $z = 1$ as compared to the suction situation (i.e., $Pe < 0$) An asymmetrical effect is depicted in the basic volumetric fraction profiles $\varphi_b(z)$ of solid nanoparticles as a consequence of the augmenting values of the control parameter $|Pe|$, in a such a way that a certain number of solid nanoparticles tends to migrate from the cold region (i.e., $z \to 1$) to concentrate more near the hot region (i.e., $z \to 0$) according to the conservative volume fraction law $\int_0^1 \varphi_b(z)dz = 0$. Besides the strengthening effect of the throughflow constraint at $z = 0$ and $z = 1$ on the nanoscale mass-transportation of solid nanoparticles within the nanofluidic medium, Fig. 5 proves that the partial migration of solid nanoparticles illustrated graphically in Fig. 4 can be reinforced more via the larger values of the Lewis numberLe.

As discussed before, the behavior of an embedded control parameter on the evolution of the stationary neutral stability curves is illustrated graphically and tabularly in Figs. 6–9 and Tables 7–10 by keeping the other background parameters fixed at specified values. Generally, it is found from these demonstrations that the blowing case (i.e., $Pe > 0$) provides higher thermal stability to the nanofluidic medium compared with the suction situation (i.e., $Pe < 0$). These findings indicate that the blowing velocity w_0 (i.e., $w_0 > 0$)crossed vertically the permeable walls $z = 0$ and $z = 1$ deferrals the appearance of convection in the medium, whilst the suction velocity (i.e., $w_0 < 0$) hastens it. Indeed, the existence of a vertically upward throughflow opposes the Brownian motion of solid nanoparticles from the higher concentration region (i.e., $z \to 1$) to the lower concentration region (i.e., $z \to 0$). As a result of this prevention in the Brownian diffusion mechanism, the nanoparticles accumulate more near the cold region (i.e., $z \to 1$) to offer relative stability to the non-homogeneous mixture. Dissimilarly, the presence of a vertically downward throughflow strengthens more the Brownian motion of nanoparticles as demonstrated in Fig. 4. For this reason, the nanofluidic system is less stable thermally in the suction configuration as compared with the blowing case, in which the critical size of convection cells $L_C(= 2\pi/a_C)$ is higher somewhat to those obtained in the blowing situation at the onset of convection. These important findings are completely authenticated via the dual behavior of the nanoparticle Rayleigh number Rn towards the stability features of the nanofluidic medium as emphasized in Fig. 6

Table 5
Comparison between the present results and those of the existing literature for the regular fluids, when $\varphi_0 = Pe = 0$.

Q	Existing Results						Present Results	
	CVM [44]		RKFM [30]		PSM [32]		CGLSM	
	Ra_C	a_C	Ra_C	a_C	Ra_C	a_C	Ra_C	a_C
0	1707.8	3.13	1707.7617	3.1163	1707.7617	3.1163	1707.7617	3.1163
100	3757.4	4.00	3757.2301	4.0120	3757.2301	4.0120	3757.2301	4.0120
200	5488.6	4.45	5488.5332	4.4458	5488.5332	4.4458	5488.5332	4.4458

Table 6
Comparison between the present results and those of the existing literature for the nanofluids, when $Rn = 0.1$, $Le = 5000$, $Nb = Nt = 10^{-6}$ and $Pe = 0$.

Q	Existing Results						Present Results	
	GDQM [31]		WGWRT [31]		PSM [32]		CGLSM	
	Ra_C	a_C	Ra_C	a_C	Ra_C	a_C	Ra_C	a_C
0	846.86042	2.43637	846.86043	2.43638	846.86043	2.43638	846.86043	2.43637
100	3091.08440	3.83812	3091.08440	3.83812	3091.08440	3.83812	3091.08440	3.83811
200	4860.63528	4.33834	4860.63528	4.33833	4860.63528	4.33833	4860.63528	4.33833

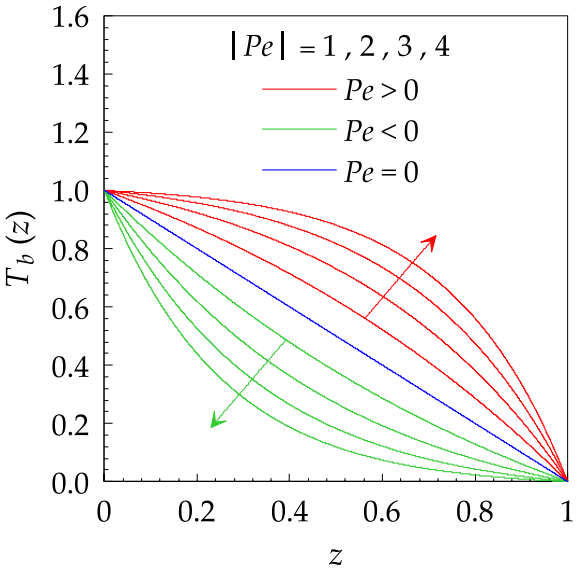

Fig. 3. Behavior of $T_b(z)$ against various values of Pe.

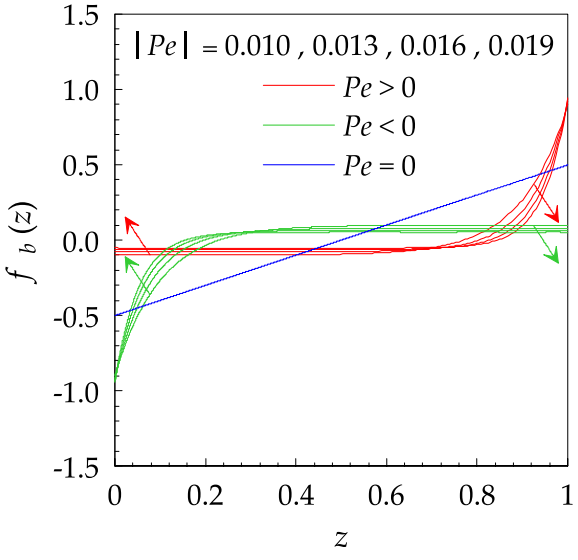

Fig. 4. Behavior of $\varphi_b(z)$ against various values of Pe.

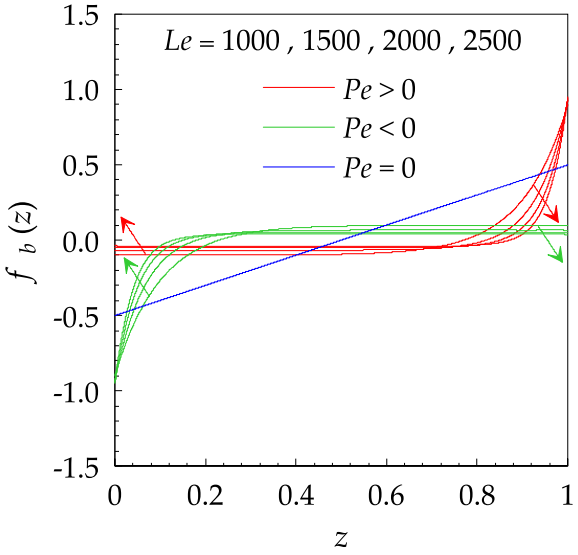

Fig. 5. Behavior of $\varphi_b(z)$ against various values of Le.

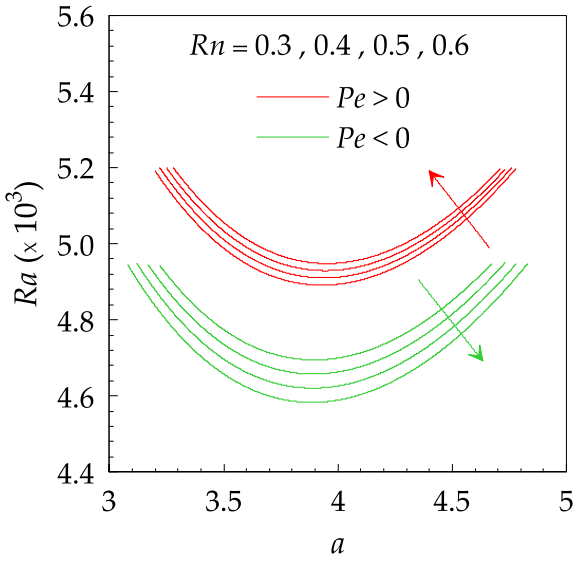

Fig. 6. Stationary marginal stability curves for increasing values of Rn.

and Table 7. Additionally, the stabilizing/destabilizing impact of the wall blowing/suction velocity w_0 is standed clearly with the increasing values of the nanoparticle Rayleigh number Rn indicating that the larger values of the initial volume fraction of solid nanoparticles φ_0 play a retarding role for the occurrence of convection cells in the medium with a lessening in their critical size L_C when the permeable walls are traversed by an upward blowing velocity w_0. A reverse trend is seen for the case of a downward suction velocity w_0. Although the blowing configuration promises a sufficient level of stability to the nanofluidic medium as compared with the suction arrangement, the heating effect of the increasing positive values of the Péclet number Pe underlined in Fig. 3 renders the thermal stability of the nanofluidic medium more sensible to any small upsurge in the temperature difference $\Delta T(= T_H - T_C)$ between the lower and the upper boundaries, which leads to destabilization in the system with an enlargement in the critical size of convection cells L_C, while the cooling effect of the suction strength contributes significantly in the thermal stability of the nanofluidic layer with a reduction in the critical size of convection cells L_C as evidenced in Fig. 7 and Table 8. Fundamentally, the electrically conducting property of the studied nanofluid gives rise to the development of magnetic Lorentz forces in the nanofluidic medium because of the mutual interaction between the induced magnetic field and the velocity of the nanofluid. These magnetic forces act oppositely on the resulting upward convective motion of the nanofluid. Due to this restive tendency of Lorentz forces, the thermal stability of the nanofluid increases remarkably with a diminishing in the critical size of convection cells L_C in both throughflow varieties as long as the

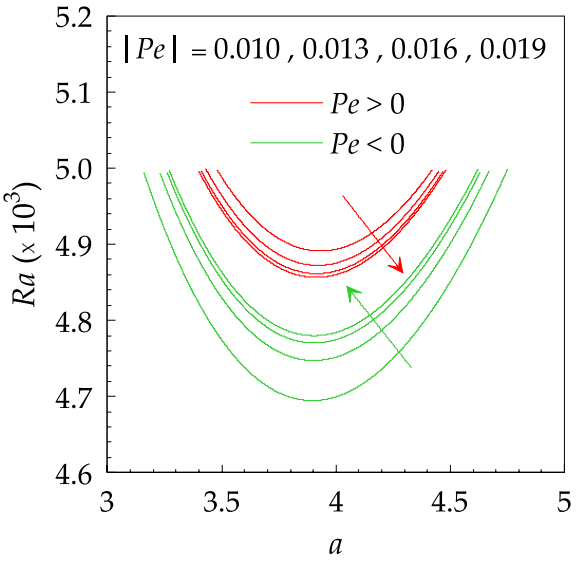

Fig. 7. Stationary marginal stability curves for increasing values of $|Pe|$.

magnetic Chandrasekhar number Q increases with a more advantageous thermal stability trend in favor of the blowing case as exposed in Fig. 8 and Table 9. Physically, an enhancement in the thermal diffusivity of the nanofluidic medium yields to an escalation in the value of Lewis number Le. Consequently, a quite reinforcement in the stabilizing/destabilizing feature of the wall blowing/suction velocity w_0 can be achieved just by intensifying the effect of Lewis number Le as shown in Fig. 9 and Table 10. This physical parameter exhibits a dual behavior, it accelerates the happening of convection cells in the blowing configuration with a slight growth in the critical size of convection cells L_C, while a postponing trend is observed in the suction situation with a decline in the critical size of convection cells L_C. Hence, the Lewis number Le affects more on the behavior of the convective part of nanoparticles mass flux added in the thermal energy equation according to the sense of the applied vertical throughflow.

5. Concluding remarks

A robustness numerical algorithm has been developed in this nanofluid stability problem to scrutinize the influence of an externally applied magnetic field on the manifestation of stationary thermo-magneto-convection that can be happened in confined nanofluidic media under the effective impact of a vertical negative temperature gradient and the presence of blowing/suction dynamical process. By adopting an improved Buongiorno's two-phase nanofluid model, the linear stability theory along with the normal mode analysis

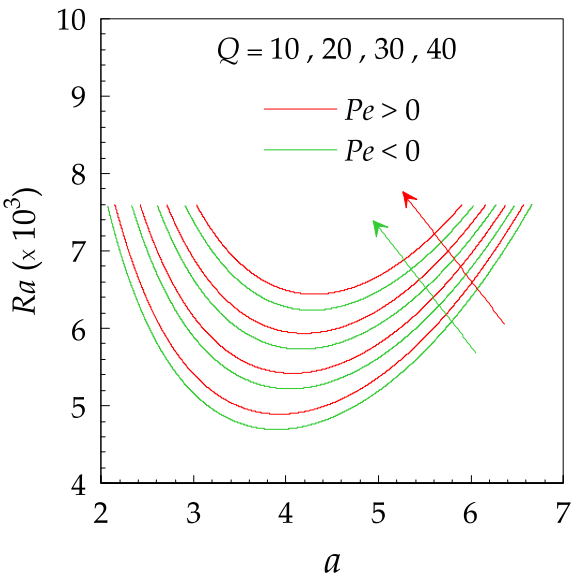

Fig. 8. Stationary marginal stability curves for increasing values of Q.

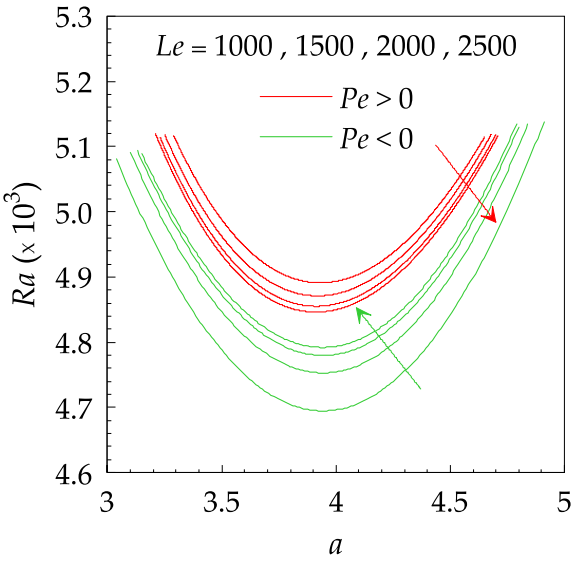

Fig. 9. Stationary marginal stability curves for increasing values of *Le*.

Table 7
Numerical CGLSM estimations of Ra_C and a_C for various values *Pe* and *Rn*.

$Rn = 0.6$		$Rn = 0.3$		*Pe*
a_C	Ra_C	a_C	Ra_C	
3.9526	4947.0470	3.9305	4890.0592	0.010
3.8853	4581.8140	3.8957	4693.3815	−0.010

Table 8
Numerical CGLSM estimations of Ra_C and a_C for various values *Pe*.

$\|Pe\| = 0.019$		$\|Pe\| = 0.010$		Case
a_C	Ra_C	a_C	Ra_C	
3.9124	4855.1790	3.9305	4890.0592	Blowing
3.9035	4778.6378	3.8957	4693.3815	Suction

Table 9
Numerical CGLSM estimations of Ra_C and a_C for various values *Pe* and *Q*.

$Q = 40$		$Q = 10$		*Pe*
a_C	Ra_C	a_C	Ra_C	
4.3044	6439.3980	3.9305	4890.0592	0.010
4.2779	6232.2795	3.8957	4693.3815	−0.010

Table 10
Numerical CGLSM estimations of Ra_C and a_C for various values *Pe* and *Le*.

$Le = 1500$		$Le = 1000$		*Pe*
a_C	Ra_C	a_C	Ra_C	
3.9190	4869.9264	3.9305	4890.0592	0.010
3.9028	4751.7396	3.8957	4693.3815	−0.010

technique has been applied properly to derive the governing stability equations analytically. These resulting differential equations were tackled thereafter numerically for the isothermal, no-slip, and zero nanoparticles mass flux conditions by employing the Chebyshev-Gauss-Lobatto Spectral Method (CGLSM). Briefly, the main outcomes of primary interest can be itemized as follows:

- The thermal stability of the medium is affected by the sense of vertical throughflow and its magnitude.
- The contribution of the convective term of the mass flux on the thermal transportation phenomenon depends greatly on the values given to the Péclet number *Pe* and Lewis number *Le*.
- The positive values of the Péclet number *Pe* show a heating effect on the nanofluidic medium, while a cooling impact is revealed for the negative values of the Péclet number *Pe*.
- The blowing configuration is more stable thermally than the suction arrangement.
- The resulting gap in thermal stability between the blowing and suction cases can be aggrandized more with the loading of nanoparticles via the intensifying values of the nanoparticle Rayleigh number *Rn*.
- The Péclet number *Pe* exhibits a dual behavior on the thermal stability of the nanofluidic medium depending on its sign.
- The stability feature of the blowing configuration diminishes with the increasing values of the parameter *Pe*. However, this thermal stability increases with the increasing values of $|Pe|$ in the suction case.
- The suction process reinforces the Brownian motion of nanoparticles, while the blowing mechanism weaknesses this kind of motion.
- The magnetic Chandrasekhar number Q has generally a stabilizing impact on the nanofluidic medium.
- The Lewis number *Le* strengthens the stabilizing/destabilizing property of the blowing/suction process.
- The critical size of convection cells L_C varies inversely with the thermal stability of the medium.

Declaration of competing interest

The authors declare that they have no known competing financial interests or personal relationships that could have appeared to influence the work reported in this paper.

Acknowledgments

The authors express their affectionate thanks to the respected Editor in chief and honorable reviewers for their valuable suggestions and comments to improve the presentation of this article.

References

[1] V.J. Rossow, On flow of electrically conducting fluids over a flat plate in the presence of a transverse magnetic field, NACA Rept 1358 (1958).
[2] H. Alfvén, Existence of electromagnetic-hydrodynamic waves, Nature 150 (1942) 405–406, https://doi.org/10.1038/150405d0.
[3] P. Pal, K. Kumar, Role of uniform horizontal magnetic field on convective flow, Eur. Phys. J. B. 85 (2012) 201, https://doi.org/10.1140/epjb/e2012-30048-8.
[4] P.P. Bulatova, V.N. Samokhin, G.A. Chechkin, Equations of magnetohydrodynamic boundary layer for a modified incompressible viscous medium. Boundary layer separation, J. Math. Sci. 232 (2018) 299–321, https://doi.org/10.1007/s10958-018-3874-1.
[5] M. Sheikholeslami, H.B. Rokni, Simulation of nanofluid heat transfer in presence of magnetic field: a review, Int. J. Heat Mass Tran. 115 (2017) 1203–1233, https://doi.org/10.1016/j.ijheatmasstransfer.2017.08.108.
[6] I.A. Mirza, M. Abdulhameed, S. Shafie, Magnetohydrodynamic approach of non-Newtonian blood flow with magnetic particles in stenosed artery, Appl. Math. Mech. 38 (2017) 379–392, https://doi.org/10.1007/s10483-017-2172-7.
[7] M. Sheikholeslami, Numerical investigation for CuO-H2O nanofluid flow in a porous channel with magnetic field using mesoscopic method, J. Mol. Liq. 249 (2018) 739–746, https://doi.org/10.1016/j.molliq.2017.11.069.
[8] K. Ahmad, A. Ishak, Magnetohydrodynamic flow and heat transfer of a Jeffrey fluid towards a stretching vertical surface, Therm. Sci. 21 (2017) 267–277, https://doi.org/10.2298/TSCI141103029A.
[9] T. Hayat, A. Aziz, T. Muhammad, A. Alsaedi, On magnetohydrodynamic three-dimensional flow of nanofluid over a convectively heated nonlinear stretching surface, Int. J. Heat Mass Tran. 100 (2016) 566–572, https://doi.org/10.1016/j.ijheatmasstransfer.2016.04.113.
[10] F.S. Ibrahim, I.A. Hassanien, A.A. Bakr, Unsteady magnetohydrodynamic micropolar fluid flow and heat transfer over a vertical porous plate through a porous medium in the presence of thermal and mass diffusion with a constant heat source, Can. J. Phys. 82 (2004) 775–790, https://doi.org/10.1139/p04-021.
[11] R. Kandasamy, K. Periasamy, K.K. Sivagnana Prabhu, Chemical reaction, heat and mass transfer on MHD flow over a vertical stretching surface with heat source and thermal stratification effects, Int. J. Heat Mass Tran. 48 (2005) 4557–4561, https://doi.org/10.1016/j.ijheatmasstransfer.2005.05.006.
[12] R. Sivaraj, I.L. Animasaun, A.S. Olabiyi, S. Saleem, N. Sandeep, Gyrotactic microorganisms and thermoelectric effects on the dynamics of 29 nm CuO-water nanofluid over an upper horizontal surface of paraboloid of revolution, Multidiscip. Model. Mater. Struct. 14 (2018) 695–721, https://doi.org/10.1108/MMMS-10-2017-0116.
[13] O.D. Makinde, I.L. Animasaun, Thermophoresis and Brownian motion effects on MHD bioconvection of nanofluid with nonlinear thermal radiation and quartic chemical reaction past an upper horizontal surface of a paraboloid of revolution, J. Mol. Liq. 221 (2016) 733–743, https://doi.org/10.1016/j.molliq.2016.06.047.
[14] O.D. Makinde, I.L. Animasaun, Bioconvection in MHD nanofluid flow with nonlinear thermal radiation and quartic autocatalysis chemical reaction past an upper surface of a paraboloid of revolution, Int. J. Therm. Sci. 109 (2016) 159–171, https://doi.org/10.1016/j.ijthermalsci.2016.06.003.
[15] K. Das, N. Acharya, P.K. Kundu, The onset of nanofluid flow past a convectively heated shrinking sheet in presence of heat source/sink: a Lie group approach, Appl. Therm. Eng. 103 (2016) 38–46, https://doi.org/10.1016/j.applthermaleng.2016.03.112.
[16] N. Acharya, K. Das, P.K. Kundu, Ramification of variable thickness on MHD TiO2 and Ag nanofluid flow over a slendering stretching sheet using NDM, Eur. Phys. J. Plus. 131 (2016) 303, https://doi.org/10.1140/epjp/i2016-16303-4.
[17] N. Acharya, S. Maity, P.K. Kundu, Framing the hydrothermal features of magnetized TiO2–CoFe2O4 water-based steady hybrid nanofluid flow over a radiative revolving disk, Multidiscip. Model. Mater. Struct. 16 (2019) 765–790, https://doi.org/10.1108/MMMS-08-2019-0151.
[18] N. Acharya, K. Das, P.K. Kundu, Effects of aggregation kinetics on nanoscale colloidal solution inside a rotating channel, J. Therm. Anal. Calorim. 138 (2019) 461–477, https://doi.org/10.1007/s10973-019-08126-7.

[19] N. Acharya, On the flow patterns and thermal behaviour of hybrid nanofluid flow inside a microchannel in presence of radiative solar energy, J. Therm. Anal. Calorim. (2019), https://doi.org/10.1007/s10973-019-09111-w.
[20] N. Acharya, R. Bag, P.K. Kundu, On the mixed convective carbon nanotube flow over a convectively heated curved surface, Heat Transf 49 (2020) 1713–1735, https://doi.org/10.1002/htj.21687.
[21] J. Buongiorno, Convective transport in nanofluids, J. Heat Tran. 128 (2006) 240–250, https://doi.org/10.1115/1.2150834.
[22] D.A. Nield, A. V Kuznetsov, The onset of convection in a horizontal nanofluid layer of finite Depth : a revised model, Int. J. Heat Mass Tran. 77 (2014) 915–918, https://doi.org/10.1016/j.ijheatmasstransfer.2014.06.020.
[23] D.A. Nield, A. V Kuznetsov, Thermal instability in a porous medium layer saturated by a nanofluid: a revised model, Int. J. Heat Mass Tran. 68 (2014) 211–214, https://doi.org/10.1016/j.ijheatmasstransfer.2013.09.026.
[24] D.A. Nield, A.V. Kuznetsov, The effect of vertical throughflow on thermal instability in a porous medium layer saturated by a nanofluid: a revised model, ASME. J. Heat Transf. 137 (2015), https://doi.org/10.1115/1.4029773, 052601:1–052601:5.
[25] A. Wakif, Z. Boulahia, F. Ali, M.R. Eid, R. Sehaqui, Numerical analysis of the unsteady natural convection MHD Couette nanofluid flow in the presence of thermal radiation using single and two-phase nanofluid models for Cu-water nanofluids, Int. J. Appl. Comput. Math. 4 (2018) 81, https://doi.org/10.1007/s40819-018-0513-y.
[26] I.L. Animasaun, R.O. Ibraheem, B. Mahanthesh, H.A. Babatunde, A meta-analysis on the effects of haphazard motion of tiny/nano-sized particles on the dynamics and other physical properties of some fluids, Chin. J. Phys. 60 (2019) 676–687, https://doi.org/10.1016/j.cjph.2019.06.007.
[27] A. Wakif, I.L. Animasaun, P.V. Satya Narayana, G. Sarojamma, Meta-analysis on thermo-migration of tiny/nano-sized particles in the motion of various fluids, Chin. J. Phys. (2019), https://doi.org/10.1016/j.cjph.2019.12.002.
[28] A. Wakif, Z. Boulahia, R. Sehaqui, Analytical and numerical study of the onset of electroconvection in a dielectric nanofluid saturated a rotating Darcy porous medium, Int. J. Adv. Comput. Sci. Appl. 7 (2016) 299–311, https://doi.org/10.14569/ijacsa.2016.070841.
[29] A. Wakif, Z. Boulahia, R. Sehaqui, A semi-analytical analysis of electro-thermo-hydrodynamic stability in dielectric nanofluids using Buongiorno's mathematical model together with more realistic boundary conditions, Results Phys 9 (2018) 1438–1454, https://doi.org/10.1016/j.rinp.2018.01.066.
[30] A. Wakif, Z. Boulahia, S.R. Mishra, M.M. Rashidi, R. Sehaqui, Influence of a uniform transverse magnetic field on the thermo-hydrodynamic stability in water-based nanofluids with metallic nanoparticles using the generalized Buongiorno's mathematical model, Eur. Phys. J. Plus. 133 (2018) 1–16, https://doi.org/10.1140/epjp/i2018-12037-7.
[31] A. Wakif, Z. Boulahia, A. Amine, I.L. Animasaun, M.I. Afridi, M. Qasim, R. Sehaqui, Magneto-convection of alumina - water nanofluid within thin horizontal layers using the revised generalized Buongiorno's model, Front. Heat Mass Transf. 12 (2019) 1–15, https://doi.org/10.5098/hmt.12.3.
[32] A. Wakif, A. Chamkha, T. Thumma, I.L. Animasaun, R. Sehaqui, Thermal radiation and surface roughness effects on the thermo-magneto-hydrodynamic stability of alumina-copper oxide hybrid nanofluids utilizing the generalized Buongiorno's nanofluid model, J. Therm. Anal. Calorim. (2020), https://doi.org/10.1007/s10973-020-09488-z.
[33] H. Mondal, A. Das, K. Kumar, Onset of oscillatory Rayleigh-Bénard magneto-convection with rigid horizontal boundaries, Phys. Plasmas 25 (2018) 12119, https://doi.org/10.1063/1.5009540.
[34] S. Das, K. Kumar, Thermal flux in unsteady Rayleigh-Bénard magnetoconvection, Int. J. Heat Mass Tran. 142 (2019) 118413, https://doi.org/10.1016/j.ijheatmasstransfer.2019.07.063.
[35] A. Wakif, Z. Boulahia, R. Sehaqui, Numerical analysis of the onset of longitudinal convective rolls in a porous medium saturated by an electrically conducting nanofluid in the presence of an external magnetic field, Results Phys 7 (2017) 2134–2152, https://doi.org/10.1016/j.rinp.2017.06.003.
[36] I.M. Afridi, M. Qasim, A. Wakif, A. Hussanan, Second law analysis of dissipative nanofluid flow over a curved surface in the presence of Lorentz force: utilization of the Chebyshev–Gauss–Lobatto spectral method, Nanomaterials 9 (2019) 1–21, https://doi.org/10.3390/nano9020195.
[37] M.K. Nayak, A. Wakif, I.L. Animasaun, M.S.H. Alaoui, Numerical differential quadrature examination of steady mixed convection nanofluid flows over an isothermal thin needle conveying metallic and metallic oxide nanomaterials: a comparative investigation, Arabian J. Sci. Eng. (2020), https://doi.org/10.1007/s13369-020-04420-x.
[38] G. Rasool, A. Wakif, Numerical spectral examination of EMHD mixed convective flow of second grade nanofluid towards a vertical riga plate using an advanced version of the revised Buongiorno's nanofluid model, J. Therm. Anal. Calorim. (2020), https://doi.org/10.1007/s10973-020-09865-8.
[39] N. Acharya, Spectral quasi linearization simulation of radiative nanofluidic transport over a bended surface considering the effects of multiple convective conditions, Eur. J. Mech. B Fluid 84 (2020) 139–154, https://doi.org/10.1016/j.euromechflu.2020.06.004.
[40] A. Wakif, A novel numerical procedure for simulating steady MHD convective flows of radiative casson fluids over a horizontal stretching sheet with irregular geometry under the combined influence of temperature-dependent viscosity and thermal conductivity, Math. Probl Eng. 2020 (2020), https://doi.org/10.1155/2020/1675350. Article ID 1675350, 20 pages.
[41] T. Thumma, A. Wakif, I.L. Animasaun, Generalized differential quadrature analysis of unsteady three-dimensional MHD radiating dissipative Casson fluid conveying tiny particles, Heat Transf 49 (2020) 2595–2626, https://doi.org/10.1002/htj.21736.
[42] C. Canuto, M.Y. Hussaini, A.M. Quarteroni, A. Thomas Jr., Spectral Methods in Fluid Dynamics, Springer Science & Business Media, 2012.
[43] L.N. Trefethen, Spectral Methods in MATLAB, SIAM, 2000.
[44] S. Chandrasekhar, Hydrodynamic and Hydromagnetic Stability, Oxford University Press, Oxford, 1961.